Molecular structure—two-photon absorption property relations in polymethine dyes

Jie Fu, Lazaro A. Padilha, David J. Hagan, and Eric W. Van Stryland

*College of Optics and Photonics: CREOL & FPCE; University of Central Florida, Orlando, FL 32816, USA,
and Department of Physics, University of Central Florida, Orlando, FL 32816, USA*

Olga V. Przhonska and Mikhail V. Bondar

Institute of Physics, National Academy of Sciences, Prospect Nauki 46, Kiev, 03028, Ukraine

Yuriy L. Slominsky and Alexei D. Kachkovski

Institute of Organic Chemistry, National Academy of Sciences, Murmanskaya 5, Kiev, 03094, Ukraine

We performed a comprehensive experimental investigation of two-photon absorption (2PA) spectra of a series of 12 symmetrical and asymmetrical cationic polymethine dyes, including complete one-and two-photon excitation anisotropy measurements. Quantum-chemical calculations were performed with the goal of understanding the nature of 2PA bands and of uncovering structure-property relations. We found that there are 2PA bands in the spectral region between the first absorption band and that for twice its energy. A weakly allowed 2PA band within the short-wavelength shoulder of the first absorption band was observed owing to the effects of vibrational and charge distribution symmetry breaking. The nature of the strongest 2PA band is connected to the electron transition from the molecular orbital localized at the benzene rings of the terminal groups to the lowest unoccupied molecular orbital (LUMO). Structure-property relations revealed that the 2PA cross section tends to be enhanced by either an increase in the length of the polymethine chromophore or an increase in the donor strengths in the terminal groups. © 2006 Optical Society of America

OCIS codes: 190.4180, 190.4710.

1. INTRODUCTION

The development of a link between molecular structure and two-photon absorption (2PA) properties of organic materials is an ongoing area of research owing to a number of promising practical applications for 2PA, ranging from bioimaging to optical data storage and 3D microfabrication (Ref. 1 and references therein). To provide this link, one must start from an understanding of the formation of one-and two-photon absorption spectra in a series of molecules with systematic changes in structure. Detailed experimental characterization combined with quantum-chemical calculations and modeling can give the necessary information for the development of a design strategy. Recent studies from various research groups have shown connections between efficient 2PA and various elements of molecular structure, such as the type and length of the conjugated chromophores, the symmetrical and asymmetrical combinations of electron donor (D) and acceptor (A) terminal groups, and the addition of such groups in the middle of the chromophore.[1–6] A design strategy for symmetrically substituted molecules with the general structure D−π−D was recently reported in Refs. 7 and 8. The values of 2PA cross sections (δ_{2PA}) had been correlated with intramolecular charge transfer from the terminal donor groups to the π-conjugated chromophore. A design strategy was directed to affect the amount of intramolecular charge transfer by increasing the length of

conjugation or by attaching electron acceptors as side groups to the π system, thus producing a D−π−A−π−D structure. Molecules based on the structure A−π−D−π−A also show large δ_{2PA}, indicating that intramolecular charge transfer is independent of the transfer direction. Most of the studies have been performed in a series of neutral π-conjugated molecules with different backbones: stilbene, distirylbenzene, polyene, diphenylpolyene, and indenofluorene.[7,8] Even though there has been considerable progress in the study of structure-property relations of organic molecules, much more remains to be discovered. Cationic polymethine dyes (PDs) are attractive candidates for 2PA studies owing to their very large ground-state to first excited-state transition dipole moments, near-parallel orientation of their ground-and excited-state transitions,[9] and sharp low-energy side of their linear absorption spectra, allowing for significant intermediate-state resonance enhancement.[10]

In this paper, we perform correlated experimental and quantum-chemical studies on a series of cationic polymethine molecules with conjugated chains of different lengths and with different terminal groups (symmetrical and asymmetrical) to provide a deeper insight into the nature of the 2PA processes and to reveal structure-property relations. In the following sections we will describe (1) the structure and one-photon absorption properties of polymethines; (2) the experimental methods used for 2PA

spectra characterization, as well as for one-and two-photon anisotropy measurements; and (3) a detailed analysis of the 2PA spectra and their quantum-chemical modeling that allows us to understand the nature of the 2PA bands. Structure-property relations in polymethines reveal the following trends: an increase of δ_{2PA} upon lengthening of the polymethine chromophore and increas-ing of the donor strength of their terminal groups.

2. EXPERIMENTAL

A. Materials
The molecular structures of PDs studied in this paper are shown in Fig. 1. Their chemical names are as follows: 2-[3-(1,3-dihydro-1,3,3-trimethyl-2*H*-indol-2-ylidene)-1-propenyl]-1,3,3-trimethyl-3*H*-indolium tetrafluoroborate (labeled as PD AF); 2-[5-(1,3-dihydro-3,3-dimethyl-1-propyl-2*H*-indol-2-ylidene)-1,3-pentadienyl]-3,3-dimethyl-1-propyl-3*H*-indolium iodide (labeled as PD 2350); 2-[7-(1,3-dihydro-3,3-dimethyl-1-phenyl-2*H*-indol-2-ylidene)-1,3,5-heptatrienyl]-3, 3-dimethyl-1-phenyl-3*H*-indolium perchlorate (labeled as PD 3428); 2-[2-[3-[(1,3-dihydro-3,3-dimethyl-1-phenyl-2*H*-indol-2-ylidene) ethylidene]-2-phenyl-1-cyclohexen-1-yl]ethenyl]-3,3-dimethyl-1-phenyl-3*H*-indolium perchlorate (labeled as PD 2093); 2-[9-(1,3-dihydro-1,3,3-trimethyl-2*H*-indol-2-ylidene)-3,7-dimethyl-4,6-(2,2-dimethyltrimethylene)-1, 3,5,7-nonatetraenyl]-1,3,3-trimethyl-3*H*-indolium perchlorate (labeled as PD 824); 2-[5-(3-ethyl-1,3-dihydro-1,1-dimethyl-2*H*-benzo-[*e*]indol-2-ylidene)-1,3-pentadienyl]-3-ethyl-1,1-dimethyl-1*H*-benzo[*e*]indolium *p*-toluensulfonate (labeled as PD 2630); 3-ethyl-2-[3-(3-ethyl-2(3*H*)benzothiazolylidene)-1-propenyl] benzo thiazolium *p*-toluensulfonate (labeled as PD 25); 3-methyl-2-[5-(3-methyl-2(3*H*)-benzothiazolylidene)-1,3-pentadienyl]benzothiazolium *p*-toluensulfonate (labeled as PD 2646); 3-ethyl-2-[5-(3-ethyl-2(3*H*)-benzothiazolylidene)-2,4-(trimethylene)-1,3-pentadienil]benzothiazolium iodide (labeled as PD 200); 3-methyl-2-[7-(3-methyl-2(3*H*)-benzothiazolylidene)-1,3,5-heptatrienyl]-benzothiazolium *p*-toluen-sulfonate (labeled as PD 2501); 3-ethyl-2-[5-(1,3-dihydro-1,3,3-trimethyl-2*H*-indol-2-ylidene)-1,3-pentadienyl] benzothiazolium perchlorate (labeled as PD 2665); and 2-[2-[4-(dimethylamino)phenyl]vinyl]-3-ethyl-1,3-benzothiazolium *p*-toluensulfonate (labeled as Styryl 1).

The linear absorption spectra of the molecules of Fig. 1, recorded with a Varian Cary 500 spectrophotometer, are shown in Figs.2–5, Fig. 7, and Fig. 8 and are discussed in Section 3. The main spectroscopic properties of the cationic PDs are determined by the existence of a delocalized π-electron system in the polymethine chromophore (or polymethine chain) and symmetric terminal groups with the exception of the weakly asymmetrical PD 2665 and strongly asymmetrical Styryl 1. All symmetrical PDs can be considered as D−π-conjugation (A)−D systems. The terminal groups, which themselves possess delocalized π-electron systems and may increase the overall conjugation chain, are thiazolium, indolium, and benzoindolium. These dyes were synthesized by standard methods as described in Ref. 11. Their molecular structures were confirmed by elemental analysis and nuclear magnetic resonance spectra.

B. Experimental Methods

1. One-Photon Excitation Fluorescence Anisotropy Spectra
One-photon excitation fluorescence anisotropy measurements, especially when linked to quantum-chemical calculations, can reveal the spectral positions and orientations of the transition dipole moments from the ground state S_0 to the first excited state S_1 ($\boldsymbol{\mu}_{01}$) and to higher excited states S_n ($\boldsymbol{\mu}_{0n}$) relative to the orientation of the emission dipole moment ($\boldsymbol{\mu}_{10}$). This information cannot be fully obtained from the linear absorption spectra. The excitation anisotropy spectrum, $r(\lambda)$, is defined as $r(\lambda) = [I_{\parallel}(\lambda) - I_{\perp}(\lambda)]/[I_{\parallel}(\lambda) + 2I_{\perp}(\lambda)]$, where $I_{\parallel}$ and $I_{\perp}$ are the fluorescence intensities polarized parallel and perpendicular to the excitation light respectively.[12]

All polymethines display two 2PA bands with $\delta_{2PA} \approx (10-600) \times 10^{-50}$ cm^4 s/photon (10−600 GM, Goppert-Mayer; 1 GM $= 1 \times 10^{-50}$ cm^{-4} s photon^{-1}), depending on dye structure, for the weak 2PA band placed near the vibronic shoulder of the first absorption band, $S_0 \rightarrow S_1$, and with $\delta_{2PA} \approx 280-2550$ GM, depending on dye structure, for the second, stronger 2PA band.

For polymethines, one-photon anisotropy values, r_{1PA}, within the first absorption band are typically close to the theoretical maximum of 0.4, indicating that $\boldsymbol{\mu}_{01}$ is almost parallel to $\boldsymbol{\mu}_{10}$. In this case, one-photon anisotropy measurements determine the mutual orientation of different absorbing dipoles, which is important for understanding 2PA processes. Steady-state one-photon excitation fluorescence anisotropy spectra of organic dyes were measured with a Photonic Technology International (PTI) Quantamaster spectrofluorimeter in high-viscosity glycerol solutions to avoid reorientation, and in low-concentration solutions ($C \approx 10^{-6}$ M) to avoid reabsorption. The angle between the absorption and emission dipole moments (β) can be determined by using $r_{1PA} = (3 \cos^2 \beta - 1)/5$. In the range $0° \leqslant \beta \leqslant 90°$, r_{1PA} values range from $-0.2 \leqslant r_{1PA} \leqslant 0.4$.

2. 2PA Spectra Measurements
Frequency-degenerate 2PA spectra of the sample solutions were measured by two methods: single-wavelength open-aperture Z scan,[13] and upconverted fluorescence.[14] In both experiments we used a Clark-MXR, CPA2010, Ti: sapphire regenerative amplified system followed by an optical parametric amplifier (Model TOPAS 4/ 800, Light Conversion) providing linearly polarized laser pulses of ≈ 140 fs (FWHM) duration at a 1 kHz repetition rate. The tuning range of the system is 520−2100 nm (0.6−2.4 eV). The Z scan allows the determination of 2PA cross sections from the fitting procedure described in Ref. 15. This method was applied to measure δ_{2PA} for the stronger second 2PA bands. The faster and more sensitive method of upconverted fluorescence was applied to measure the weak 2PA band within the first linear absorption band, which is only slightly allowed for symmetrical PDs (C_{2v}).
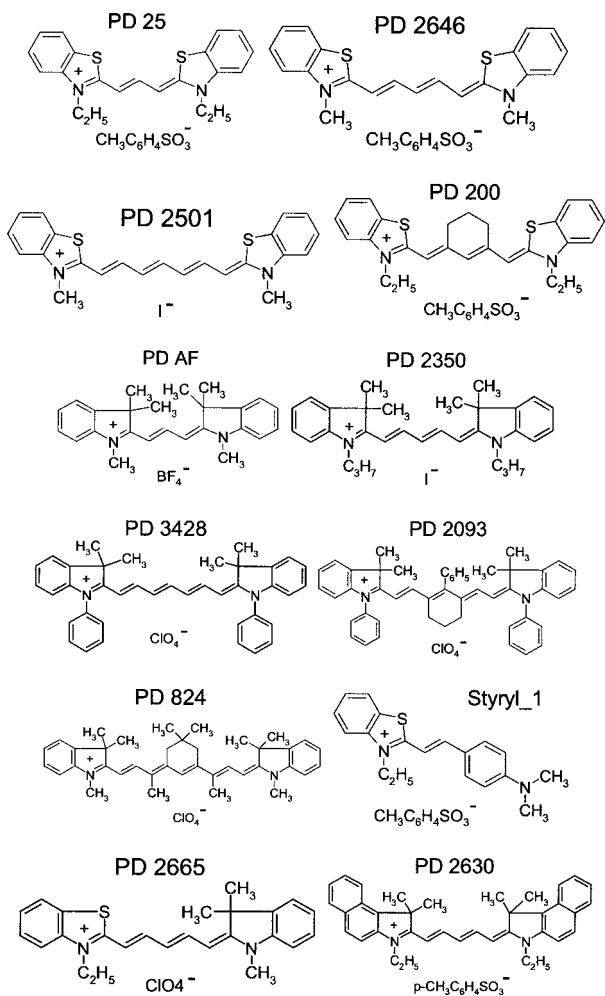
Fig. 1.   Molecular structures of PDs.

Upconverted fluorescence of the molecules was measured in a 10 mm quartz cuvette with the same PTI Quantamaster spectrofluorimeter. Fluorescence quantum yields of PDs in solutions were measured by using a standard method[14] relative to Rhodamine 6G (quantum yield is 0.96 in ethanol; see Ref. 16). The 2PA cross sections were measured and calibrated against well-known reference standards: Fluorescein in water (pH=11) and Rhodamine B in methanol.[14]

3. Two-Photon Excitation Anisotropy Spectra
Two-photon anisotropy measurements were also performed with the PTI Quantamaster spectrofluorimeter by using linearly polarized excitation from the same femtosecond laser system described in the previous section. Two-photon anisotropy values, r_{2PA}, can be measured in the same way as r_{1PA}; however, the excitation wavelength used is two times larger, denoted here as 2λ: $r_{2PA}(2\lambda)$ $=[I_{\parallel}(2\lambda)-I_{\perp}(2\lambda)]/[I_{\parallel}(2\lambda)+2I_{\perp}(2\lambda)]$. Special care was taken to minimize reabsorption of the emission, which can decrease the anisotropy owing to the effect of energy transfer.[12] This is especially important for the PDs that show a small Stokes shift of $\approx 15-20$ nm due to a large overlap of the absorption and emission spectra. We compared the shapes of upconverted fluorescence (usually redshifted owing to the high concentration typically used

for 2PA studies) with the shapes of one-photon fluorescence obtained from solutions diluted down to $\approx 10^{-6}$ M. We found that for all the molecules studied the reabsorption of upconverted fluorescence at $C \leqslant 10^{-5}$ M is negligible. Therefore, we used 10^{-5} M or smaller concentrations for all two-photon anisotropy studies. More detailed information can be found in Ref. 17, in which it was shown that by using a three-level model (initial, final, and one intermediate), one can calculate r_{2PA} values as follows:

$$r_{2PA} = \frac{18\cos(\gamma-\beta)\cos\beta\cos\gamma - 7\cos^2\gamma + 1}{7(2\cos^2\gamma + 1)}. \quad (1)$$

Here γ is the angle between dipole moments participating in the 2PA process, and β is the angle between the absorption $S_0 \rightarrow S_1$ and the emission $S_1 \rightarrow S_0$ dipoles, which can be found from one-photon anisotropy measurements. Our measurements indicate that for all the molecules studied, except for the strongly asymmetrical Styryl 1, $r_{2PA} \approx 0.48-0.5$ in the broad spectral range coverting all 2PA bands measured. For Styryl 1, $r_{2PA} \approx 0.56-0.58$ and is also wavelength independent.

Experimental results for 2PA spectra are shown in Figs.2–5, Fig. 7, and Fig. 8, and Tables 1–5, including the one- and two-photon anisotropy values (Figs. 7 and 8), and are discussed in Section 3.

C. Methodology of Quantum-Chemical Calculations
Quantum-chemical calculations were performed with the goal of understanding the nature of 2PA bands and revealing their structure-property relations. The well-known MOLCAO (Molecular Orbital as a Linear Combination of Atomic Orbitals) method was used for calculations of the positions of the electronic levels and the shapes of the molecular orbitals. The wavefunction of the ith molecular orbital (MO) φ_i, was written as a expansion of the atomic orbitals χ_μ: $\varphi_i = \Sigma_\mu C_{i\mu}\chi_\mu$, where $C_{i\mu}$ are the corresponding orbital amplitudes and the summation runs over all atomic orbitals. Here $C_{i\mu}^2$ is the probability that an electron in the ith MO is in the neighborhood of the μth atom.[18] Calculations were performed in the framework of the standard semiempirical approximations (HyperChem package). The equilibrium molecular geometries were calculated by employing the Austin Model 1 (AM1) method with the gradient 0.05 kcal/mol. It was established previously that the lengths of the carbon–carbon bonds calculated in this method are in good agreement with the corresponding values obtained by an *ab initio* approximation.[19] The π system of all molecules was found to be planar. Characteristics of the electron transitions were obtained in the ZINDO/S approximation with spectral parameterization. The wavefunction of the pth excited state Ψ_p was built as an expansion of the electron configurations $\Phi_{i \rightarrow j}$ corresponding to electron transfer from the occupied ith to the vacant jth orbital: $\psi_p = \Sigma_{i,j} T_{p,i \rightarrow j} \Phi_{i \rightarrow j}$, where $T_{p,i \rightarrow j}$ are the normalized amplitudes and indices i and j run over all MOs.[18] Note that $\Sigma_{i,j} T_{p,i \rightarrow j}^2 = 1$ is the normalization condition. The transition dipole moments from the first excited state (intermediate state) to the final state (for details see Subsection 3.D) were calculated by taking into account the fact that ex-

cited states are practically "pure" with $T_{p,i \to j} \geq 0.9$ (see Ref. 20) in the area of interest (i.e., between the linear absorption peak and that at twice this energy). In our calculations we used all $\pi \to \pi^*$ single excited configurations; the overlap weight factor (OWF) ranges from 0.26 to 0.45 to adjust the calculated positions of the $S_0 \to S_1$ bands with the experimental data. All calculations were performed on isolated molecules, neglecting solvent effects.

3. EXPERIMENTAL RESULTS AND DISCUSSION

A. Effect of the Conjugation Length

Figures 2 and 3 represent two series of PDs with thiazolium (from $n=1$ to $n=3$) and indolium (from $n=1$ to $n=4$) terminal groups, respectively. It is commonly known that an increase in the length of the polymethine chromophore by one chain unit (n) at the same terminal groups leads to a redshift in the peak of the linear absorption of about 100 nm. Introduction of the bridges (or partial cyclization of the chain) with the goal of increasing the photochemical stability, depending on the position of cyclization, leads to blueshifts (compare PDs 2646 and 200) or redshifts (compare PDs 3428 and 2093) of the absorption peaks relative to the unbridged chromophores. Values of transition dipole moments μ_{01} for the molecules, presented in Tables 1 and 2, were calculated from the integrated linear absorption band $S_0 \to S_1$ (see Ref. 4):

$$\mu_{01} = \{[1500(\hbar c)^2 \ln 10] \int \varepsilon_{01}(\nu) \mathrm{d}\nu / \pi N_A E_{01}\}^{1/2},$$

where $\varepsilon_{01}(\nu)$ is the extinction coefficient, N_A is Avogadro's number, and E_{01} is the peak energy. Calculations show that an increase in the chain length leads to an increase in the dipole moment from 10.5 D ($n=1$) to 16.8 D ($n=3$) for thiacarbocyanines in Table 1 and from 12.2 D ($n=1$) to 16.8 D ($n=4$) for indocarbocyanines in Table 2. Broadening of the linear absorption band for PD 824 ($n=4$) in the polar ethanol solution is connected with partial ground-state symmetry breaking and the appearance of a form of the molecule with an asymmetrical distribution of the
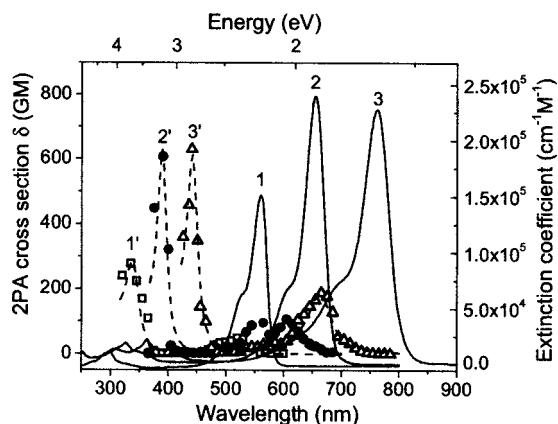
Fig. 2. Linear (1, 2, 3) and 2PA (1′, 2′, 3′) spectra for polymethine dyes with thiazolium terminal groups in ethanol: PD 25 (1, 1′, open squares); PD 2646 (2, 2′, solid circles); PD 2501 (3, 3′, open triangles). Dashed lines are theoretical fittings based on Eq. (2). For comparison with linear absorption, 2PA spectra are presented as a function of half the excitation wavelength $\lambda_{\mathrm{exc}}/2$.
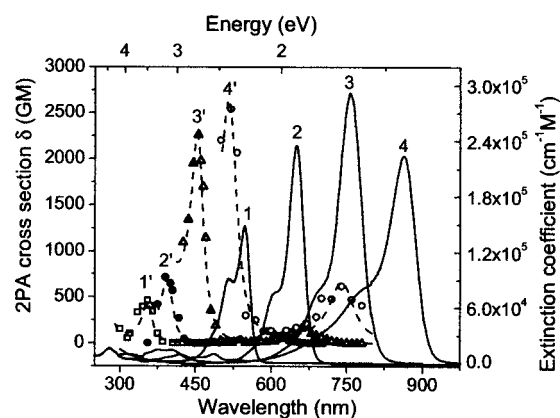
Fig. 3. Linear (1, 2, 3, 4) and 2PA (1′, 2′, 3′, 4′) spectra for polymethine dyes with indolium terminal groups in ethanol: PD AF (1, 1′, open squares); PD 2350 (2, 2′, solid circles); PD 3428 (3, 3′, open triangles); PD 824 (4, 4′, open circle). Dashed lines are theoretical fittings based on Eq. (2). For comparison with linear absorption, 2PA spectra are presented as a function of half the excitation wavelength $\lambda_{\mathrm{exc}}/2$.

Table 1. Measured and Calculated Parameters for PDs 25, 2646, and 2501 with Different Conjugation Lengths[a]

Parameter	PD		
	25 ($n=1$)	2646 ($n=2$)	2501 ($n=3$)
λ_{1PA}^{max} (nm)	560	654	760
μ_{01}^{exp} (D)	10.5	14	16.8
μ_{01}^{qchem} (D)	10.7	12.4	13.4
λ_{2PA}^{max} (nm) First band	515	585	655
δ_{2PA}^{max} (GM) First band	50	100	200
λ_{2PA}^{max} (nm) Second band	332	385	440
δ_{2PA}^{max} (GM) Second band	280	600	630
μ_{1f}^{fit} (D)	2.05	1.5	1.0
μ_{1f}^{qchem} (D)	1.5	1.4	1.6
Detuning energy (eV)	0.36	0.29	0.32

[a]n, number of repeated units in the chain; λ_{1PA}^{max} and λ_{2PA}^{max}, wavelength of the maxima of the one-photon absorption (1PA) and two-photon absorption (2PA). For comparison with linear absorption λ_{2PA}^{max} are presented as a function of $\lambda_{\mathrm{exc}}/2$, where λ_{exc} is the excitation wavelength; μ_{01}^{exp} and μ_{01}^{qchem}, ground-state transition dipole moments from experimental data and quantum-chemical calculations; δ_{2PA}^{max}, 2PA cross section (experimental uncertainties ±20%); μ_{1f}^{fit} and μ_{1f}^{qchem}, excited-state transition dipole moments from fitting based on Eq. (2) and quantum-chemical calculations.

charge density. Detailed information on our experimental and theoretical investigations of this symmetry breaking effect can be found in Ref. 21.

Two-photon absorption measurements for all PDs show the existence of two bands. First, a weakly allowed 2PA band is always positioned within the shoulder of the first absorption band $S_0 \to S_1$ when plotted as, for example, in Figs. 2 and 3. Second, a more intensive 2PA band is positioned in a shorter-wavelength region. Experimental results demonstrate that lengthening of the polymethine

Table 2. Measured and Calculated Parameters as Defined in Table 1 for PDs AF, 2350, 3428, and 824 with Different Conjugation Lengths

	PD			
Parameter	AF ($n=1$)	2350 ($n=2$)	3428 ($n=3$)	824 ($n=4$)
λ_{1PA}^{max} (nm)	547	650	756	862
μ_{01}^{exp} (D)	12.2	14.7	16.8	16.8
μ_{01}^{qchem} (D)	10.2	12.4	13.8	12.4
λ_{2PA}^{max} (nm) First band	490	590	665	740
δ_{2PA}^{max} (GM) First band	10	140	180	600
λ_{2PA}^{max} (nm) Second band	355	390	453	520
δ_{2PA}^{max} (GM) Second band	470	720	2280	2550
μ_{1f}^{fit} (D)	2.8	2.0	2.75	2.9
μ_{1f}^{qchem} (D)	3.4	3.9	2.3	2.3
Detuning energy (eV)	0.51	0.31	0.26	0.25

chromophore generally results in an increase in the 2PA cross section δ_{2PA} (see Figs. 2 and 3 and data in Tables 1 and 2). For the weak 2PA bands in the thiazolium series, δ_{2PA} increases from 50 GM for PD 25 ($n=1$) to 200 GM for PD 2501 ($n=3$), and in the indolium series from ≈ 10 GM for PD AF ($n=1$) to 600 GM for PD 824 ($n=4$). For the more intense 2PA band, δ_{2PA} in the thiazolium series increases from 280 GM for PD 25 ($n=1$) to 630 GM for PD 2501 ($n=3$) and in the indolium series from 470 GM for PD AF ($n=1$) to 2550 GM for PD 824 ($n=4$). This increase of δ_{2PA} with lengthening of the polymethine chromophore may be explained by the corresponding increase of the ground-state transition dipole moments and a decrease of the detuning energies (between excitation wavelength and intermediate S_1 state). We note that the bridged structures (PD 200, PD 2093) are characterized by smaller values of δ_{2PA} in the first 2PA band (see Table 5). Possible explanations for this will be discussed in Subsection 3.E.

B. Effect of the Terminal Groups

Next we consider the effect of the terminal groups thiazolium, indolium, and benzoindolium on one- and two-photon absorption properties. Figure 4 represents experimental data for PDs with the same length of the chromophore $n=2$ and different terminal groups placed in order of increasing donor strength: PD 2646 (thiazolium), PD 2350 (indolium), and PD 2630 (benzoindolium), respectively. These terminal groups contain their own π-conjugated system. All linear and nonlinear parameters for PDs 2646 and 2350 are very similar with respect to donor strength and contribution of π conjugation from their terminal groups to the polymethine chain. However, we note that 2PA cross section δ_{2PA} in both 2PA bands is 20%–40% larger for PD 2350 than for PD 2646 (see Table 3). For PD 2630, with a larger π conjugation (larger contribution to the chain) and increased donor strength in

the benzoindolium terminal groups, the positions of the one- and two-photon absorption peaks are redshifted, and δ_{2PA} for the second band is $\approx 1.5\times$ larger than that for PD 2646. The 2PA spectrum for PD 2630 is more complicated than that for PD 2350. In contrast to PD 2350, a beginning of the next (third) 2PA band is seen for PD 2630, with δ_{2PA} reaching 1320 GM. Further tuning of the excitation wavelength into the short-wavelength region was restricted by the presence of linear absorption. We conclude that for PDs of the same chain length, an increase of the donor strength in the terminal groups leads to an increase of 2PA cross section δ_{2PA}.
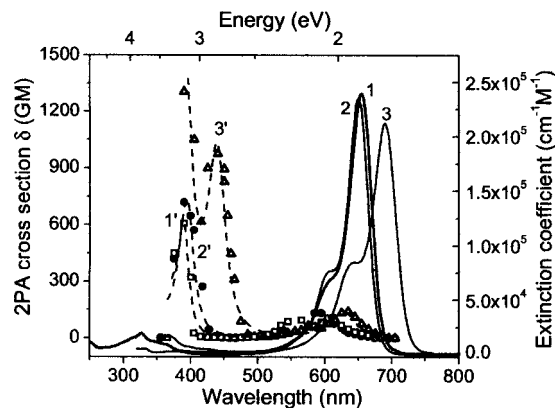
Fig. 4.   Linear (thicker curves 1, 2, 3) and 2PA ($1'$, $2'$, $3'$) spectra for polymethine dyes with the same conjugated length ($n=2$) in ethanol: PD 2646 ($1,1'$, open squares); PD 2350 ($2,2'$, solid circles); PD 2630 ($3,3'$, open triangles). Dashed lines are theoretical fittings based on Eq. (2). For comparison with linear absorption, 2PA spectra are presented as a function of half the excitation wavelength $\lambda_{exc}/2$.

Table 3. Measured and Calculated Parameters as Defined in Table 1 for PDs 2646, 2350, and 2630 with Different Terminal Groups[a] and Same Conjugation Chain Length ($n=2$)

	PD		
Parameter	2646 (Thiazolium)	2350 (Indolium)	2630 (Benzoindolium)
λ_{1PA}^{max} (nm)	654	650	690
μ_{01}^{exp} (D)	14	14.7	14.1
μ_{01}^{qchem} (D)	12.4	12.4	11.2
λ_{2PA}^{max} (nm) First band	585	590	630
δ_{2PA}^{max} (GM) First band	100	140	150
λ_{2PA}^{max} (nm) Second band	385	390	440
δ_{2PA}^{max} (GM) Second band	600	720	900
μ_{1f}^{fit} (D)	1.5	2.0	3.1
μ_{1f}^{qchem} (D)	1.4	3.9	3.0
Detuning energy (eV)	0.29	0.31	0.38

[a]Terminal groups are in parentheses.

C. Effect of Molecular Symmetry

We consider the effect of molecular symmetry by comparing results for the symmetrical PD 2350 (indolium terminal groups, $n=2$) with those for the weakly asymmetrical PD 2665 (indolium–thiazolium terminal groups, $n=2$) as well as comparing results for the symmetrical PD 25 (thiazolium terminal groups, $n=1$) with those for the strongly asymmetrical Styryl 1 (thiazolium–styryl terminal groups, $n=1$). Experimental data are presented in Figs. 5(a) and 5(b) and Table 4. It is commonly known that asymmetrical dyes are characterized by blueshifted and broader linear absorption bands $S_0 \rightarrow S_1$ as compared with those for symmetrical dyes. Absorption shapes for asymmetrical molecules strongly depend on solvent polarity, which is connected to charge localization. The 2PA spectra also show some differences. As was expected, for the strongly asymmetrical Styryl 1, the first 2PA band is much broader and almost twice as intense as that for the symmetrical PD 25; however, δ_{2PA} for the second band is somewhat smaller. The same, but less pronounced, effect was observed for the weakly asymmetrical dye PD 2665 when compared with the symmetrical PD 2350. We note

(a)

(b)
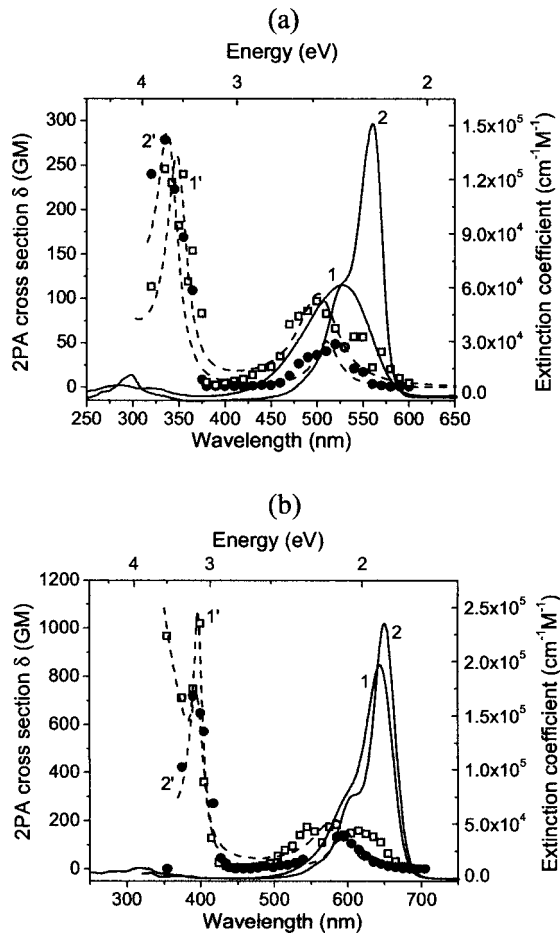
Fig. 5. (a) Linear (1, 2) and 2PA (1′, 2′) spectra for PD 25 (2, 2′, solid circles) and Styryl 1 (1, 1′ open squares) in ethanol. (b) Linear (1, 2) and 2PA (1′, 2′) spectra for PD 2350 (2, 2′, solid circles) and PD 2665 (1, 1′, open squares) in ethanol. Dashed lines are theoretical fittings based on Eq. (2). For comparison with linear absorption, 2PA spectra are presented as a function of half the excitation wavelength $\lambda_{exc}/2$.

Table 4. Measured and Calculated Parameters as Defined in Table 1 for Symmetric Molecules PDs 25 and 2350 and for Asymmetric Molecules Styry1_1 and PD 2665

Parameter	PD			
	25 ($n=1$)	Styry1_1 ($n=1$)	2350 ($n=2$)	2665 ($n=2$)
λ_{1PA}^{max} (nm)	560	527	650	643
μ_{01}^{exp} (D)	10.5	11.6	14.7	14
μ_{01}^{qchem} (D)	10.7	10.7	12.4	12.6
λ_{2PA}^{max} (nm) First band	515	500	590	585
δ_{2PA}^{max} (GM) First band	50	100	140	200
λ_{2PA}^{max} (nm) Second band	332	335	390	400
δ_{2PA}^{max} (GM) Second band	280	250	720	1000
μ_{1f}^{fit} (D)	2.05	2.5	2.0	1.75
μ_{1f}^{qchem} (D)	1.5	2.4	3.9	1.7
Detuning energy (eV)	0.36	≈0.38	0.31	0.37

Table 5. Measured and Calculated Parameters as Defined in Table 1 for Bridged Molecules PDs 200 and 2093 and for Unbridged Molecules PDs 2646 and 3428

Parameter	PD			
	200 ($n=2$)	2646 ($n=2$)	2093 ($n=3$)	3428 ($n=3$)
λ_{1PA}^{max} (nm)	648	654	770	756
μ_{01}^{exp} (D)	10.8	14	15.9	16.8
μ_{01}^{qchem} (D)	11.8	12.4	12.9	13.8
λ_{2PA}^{max} (nm) First band	580	585	670	665
δ_{2PA}^{max} (GM) First band	55	100	60	180
λ_{2PA}^{max} (nm) Second band	390	385	460	453
δ_{2PA}^{max} (GM) Second band	700	600	1200	2280
μ_{1f}^{fit} (D)	2.2	1.5	2.45	2.75
μ_{1f}^{qchem} (D)	1.1	1.4	1.3	2.3
Detuning energy (eV)	0.32	0.29	0.26	0.26

that for PD 2665 the beginning of the third 2PA band is observed, whereas this is not the case for the symmetrical PD 2350.

D. 2PA Spectra Calculations

We reproduced the shape of the 2PA spectra for all the dyes by using the experimental and calculated molecular parameters shown in Tables 1–5 and by considering a

simple extension of the three-level model proposed in Ref. 22. This model includes two final states (*f*1 and *f*2) and the same initial S_0 (0) and intermediate S_1 (1) states. Assuming that transition dipole moments $\boldsymbol{\mu}_{01}$ and $\boldsymbol{\mu}_{1f}$ are parallel to each other, the equation for δ_{2PA} at the excitation laser frequency ν_p is

$$\delta_{2PA}(\nu_p) = \frac{64\pi^3}{5c^2h} \frac{E_p^2}{(E_{01}-E_p)^2 + \Gamma_{01}^2} \left[\frac{|\boldsymbol{\mu}_{01}|^2|\boldsymbol{\mu}_{1f1}|^2\Gamma_{0f1}}{(E_{0f1}-2E_p)^2 + \Gamma_{0f1}^2} \right.$$
$$\left. + \frac{|\boldsymbol{\mu}_{01}|^2|\boldsymbol{\mu}_{1f2}|^2\Gamma_{0f2}}{(E_{0f2}-2E_p)^2 + \Gamma_{0f2}^2} \right], \qquad (2)$$

where c is the speed of light; h is Planck's constant; $E_p = h\nu_p$, $E_{01} = h\nu_{01}$, $E_{0f1} = h\nu_{0f1}$, and $E_{0f2} = h\nu_{0f2}$ are the corresponding transition energies, and Γ is a damping constant. As was noted in Ref. 10, if $1/2\nu_{0f2}$ is close to ν_{01}, simultaneous one- ($\nu_p \approx \nu_{01}$) and two-photon ($2\nu_p \approx \nu_{0f}$) resonances occur, leading to a dramatic enhancement of δ_{2PA}. Therefore, we can conclude that to obtain the largest 2PA, one should direct the molecular design toward the experimental realization of these simultaneous resonances. This has been achieved in the squaraine dyes, which display a third and more intense 2PA band with $\delta_{2PA} \geq 8600$ GM.[20] This peak is observable just below the linear absorption edge.

All calculated spectra are presented in Figs. 2–5 and Figs. 7 and 8 and show a relatively good correlation with the measured 2PA.

E. Nature of 2PA Bands

1. Nature of the Strongest 2PA Bands
Quantum-chemical calculations have been performed with the goal of understanding the 2PA spectra for cationic polymethines and to uncover their structure-property relations. First, we consider the nature of the strongest 2PA bands. For this purpose we analyzed the evolution of the electron levels and transitions from the unsubstituted polymethine chain: H_2C^+—$(CH\!=\!CH)_2$—$CH\!=\!CH_2$ to PDs with different molecular structures. The results for the unsubstituted polymethine chain and PD 2350 are summarized in Table 6. In our analysis we limited the number of levels by the number of electron transitions participating in one- and

two-photon absorption between $S_0 \rightarrow S_1$ and that for twice this energy or "double-resonance" position as described in Ref. 20.

Quantum-chemical calculations of the unsubstituted polymethine chain show that the ground to the first excited-state transition $S_0 \rightarrow S_1$ is allowed by symmetry rules $(1A_1 \rightarrow 1B_1)$ and is connected with the electron transfer between the highest occupied molecular orbital (HOMO) and the lowest unoccupied molecular orbital (LUMO). The two next electron transitions, $S_0 \rightarrow S_2$ $(1A_1 \rightarrow 2A_1)$ and $S_0 \rightarrow S_3$ $(1A_1 \rightarrow 3A_1)$, are nearly forbidden by symmetry and correspond to the transitions HOMO-1 $\rightarrow$LUMO and HOMO$\rightarrow$LUMO$+1$, respectively, with quite different oscillator strengths (see Table 6; almost 1 order of magnitude difference[20]). These transition energies are close but not exactly equal to each other. The calculated spectral shift between the corresponding $S_0 \rightarrow S_2$ and $S_0 \rightarrow S_3$ absorption bands is ≈ 20 nm, i.e., no degeneracy. One of these $A_1 \rightarrow A_1$ transitions corresponds approximately to the double-resonance position of the main absorption band (see Table 6), which makes it impossible to reach the 2PA peak experimentally, owing once more to linear absorption. All molecular orbitals in the unsubstituted conjugated polymethine chain are totally and uniformly delocalized, and all electron transitions are described mainly by single configurations with the coefficients $T_{p,i\rightarrow j} > 0.9$ (see Table 6).

Introduction of the donor terminal groups, such as indolium, benzoindolium, and thiazolium, to the polymethine chain significantly increases the density of occupied molecular orbitals, and thus the number of electronic transitions between the first band $S_0 \rightarrow S_1$ and its double-resonance position, which is the subject of interest. For substituted symmetrical PDs, for example, PD 2350 in Table 6, we can distinguish between two types of molecular orbitals. The first is connected with π delocalization, typically not only along the polymethine chain but also through the terminal groups, which causes considerable lengthening of the chromophore. The second type of orbital is characterized by charge localization on some molecular fragments. Introduction of the symmetrical terminal groups leads to formation of doubly degenerate configurations, resulting in the splitting of their energies. As a result, one configuration may be coupled with the

Table 6. Calculated Parameters for the Unsubstituted Polymethine Chain and One Typical Polymethine Dye PD 2350

Dye	Transition	λ (nm)	Oscillator Strength	Symmetry of Final State	Main Configuration
Unsubstituted chain	$S_0 \rightarrow S_1$	551	1.65	B_1	$0.96|H\rightarrow L\rangle$
	$S_0 \rightarrow S_2$	315	0.002	A_1	$0.97|H-1\rightarrow L\rangle$
	$S_0 \rightarrow S_3$	291	0.08	A_1	$0.97|H\rightarrow L+1\rangle$
PD 2350	$S_0 \rightarrow S_1$	655	1.6	B_1	$0.96|H\rightarrow L\rangle$
	$S_0 \rightarrow S_2$	460	0.01	A_1	$0.94|H-1\rightarrow L\rangle$
	$S_0 \rightarrow S_3$	410	0.07	B_1	$0.92|H-2\rightarrow L\rangle$
	$S_0 \rightarrow S_4$	395	0.02	A_1 (local)	$0.95|H-3\rightarrow L\rangle$
	$S_0 \rightarrow S_5$	386	0.06	B_1	$0.93|H-4\rightarrow L\rangle$
	$S_0 \rightarrow S_6$	352	0.05	A_1	$0.95|H\rightarrow L+1\rangle$

chain configuration, forming a delocalized molecular orbital (HOMO−2 for PD 2350 in Table 6). The second configuration remains localized at the terminal groups (or their fragments). For most of the dyes studied in this paper, this configuration corresponds to HOMO−3 with the charge localization mainly at the benzene rings of the terminal groups. The existence of this local molecular orbital is of great importance for the 2PA. Our understanding is that the localized–delocalized electron transition, such as HOMO−3→LUMO for PD 2350 in Table 6, which appears in the energy interval between $S_0 \to S_1$ and its double resonance, is responsible for the strong 2PA. A relatively high 2PA cross section δ_{2PA} can be observed owing to a strong coupling of the boundary orbitals HOMO−3 and LUMO with the intermediate HOMO.

Exceptions are PD 3428 and PD 2093, whose molecular structures contain the phenyl substituents at the nitrogen atoms of the terminal groups (see Fig. 1). Calculations show that for these molecules, HOMO−3 is localized at the phenyl rings oriented perpendicular to the molecular plane. Therefore, the electron transitions involving these orbitals cannot be active in absorption spectra. The local orbital corresponding to charge localization at the benzene rings of the terminal groups becomes HOMO−5, and thus electron transitions active in 2PA for PD 3428 and PD 2093 become HOMO−5→LUMO.

Quantum-chemical analysis enables us to conclude that for all the PDs studied, the localized unoccupied molecular orbitals are in much higher energy positions and do not participate in transitions in the spectral region of interest.[20] We note that LUMO extends the chain conjugation only to the nitrogen atoms of the terminal groups, while the π-electron conjugation at HOMO is spread out over the entire molecule.

To further increase the density of the occupied molecular orbitals and thus the number of 2PA transitions, we can choose terminal groups with a more extended π system. This idea was realized in PD 2630 ($n=2$), which contains the more complicated benzoindolium terminal groups. As compared with PD 2350 ($n=2$), this dye is characterized by redshifted absorption bands. Note that experimentally the main one-photon absorption peak is shifted by ≈ 0.1 eV and that the 2PA band is shifted more to the red by ≈ 0.18 eV. Because of this shift, the beginning of the next (third) 2PA band has been experimentally measured. Analyzing the evolution of 2PA bands from the unsubstituted chain to PD 2350, and then to PD 2630, we assume the terminal groups play a dominating role in shifting the peak of the 2PA band to a region reachable for 2PA between the first band $S_0 \to S_1$ and its double resonance, i.e., the linear absorption remains negligible for this measurement. More extended terminal groups can provide an additional shift, thereby increasing the number of reachable 2PA bands.

2. Nature of the Weakly Allowed 2PA Bands
Now we consider the nature of the weakly allowed 2PA bands that are positioned within the shoulder of the first absorption band $S_0 \to S_1$ when plotted as, for example, in Figs. 2 and 3. Two-photon excitation to the S_1 state involves a minimum of two dipole moments: $\boldsymbol{\mu}_{01}$ and $\boldsymbol{\Delta\mu}$ (vector difference between permanent S_0 and S_1 dipole
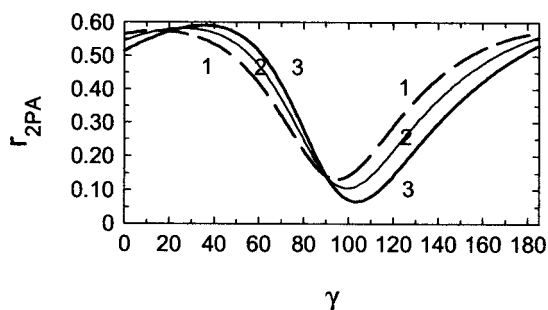
Fig. 6. Graph of two-photon excitation fluorescence anisotropy as a function of the angle between $\boldsymbol{\mu}_{01}$ and $\boldsymbol{\Delta\mu}$ at different values of β: $\beta=5°(1)$, $\beta=10°(2)$, $\beta=15°(3)$.

moments). According to traditional quantum-chemical theories,[18] 2PA to the S_1 state is symmetry forbidden for 2PA in centrosymmetric molecules, such as squaraines with C_{2i} symmetry ($\boldsymbol{\Delta\mu}=0$), and is only slightly allowed for symmetrical PDs with $C_{2\nu}$ symmetry ($\boldsymbol{\Delta\mu}$ is oriented perpendicular to $\boldsymbol{\mu}_{01}$). However, these bands have been observed for cyanines and cyaninelike molecules (squaraines, Rhodamine B, Fluorescein) and explained by the effect of symmetry breaking due to vibronic coupling, which can lead to a change of the dipole selection rules, resulting in the appearance of a 2PA band within the $S_0 \to S_1$ absorption band.[14,23]

An indication of some form of symmetry breaking was also observed by two-photon excitation fluorescence anisotropy measurements discussed in Subsection 2.B.3, which show relatively high and nearly constant values over the entire spectral range studied.[17] These results can be explained by taking into account the deviation of $\boldsymbol{\Delta\mu}$ from being perpendicular to $\boldsymbol{\mu}_{01}$. One-photon anisotropy spectra indicate that for all molecules $r_{1PA}=0.37-0.39$ within the first absorption band, indicating that the angle β between $\boldsymbol{\mu}_{01}$ and $\boldsymbol{\mu}_{10}$ does not exceed 15°. Equation (1) for r_{2PA} is presented in Subsection 2.B.3 and is shown graphically in Fig. 6 for $\beta=5°$, 10°, and 15°. From quantum-chemical analysis we can estimate that the angle γ between ground-state transition dipole moment $\boldsymbol{\mu}_{01}$ and $\boldsymbol{\Delta\mu}$ is equal to 90°, making $r_{2PA} \sim 0.14$ based on Eq. (1). However, we experimentally observed $r_{2PA} \approx 0.5$. The symmetry breaking effect leads to a reorientation of the $\boldsymbol{\Delta\mu}$ dipole difference from perpendicular to $\boldsymbol{\mu}_{01}$ by 32°, which leads to $r_{2PA} \approx 0.5$ from Fig. 6. Two-photon anisotropy spectra measurements indicate the existence of symmetry breaking in the symmetric molecules.

Our current and ongoing studies of 2PA spectra in this series of PDs with different chain lengths made it possible to assume that processes other than vibronic coupling can break the symmetry of the molecules. The frequency of the chain skeleton vibration observed in the linear absorption of PDs is $\approx 1450-1500$ cm^{-1} and is almost chain-length independent. However, in 2PA we observe a different trend. For the shorter molecules, the peak 2PA position corresponds approximately to the 1PA vibrational shoulder (again plotting as in, for example, Figs. 2 and 3), but for the longer PDs, the 2PA peak is more blueshifted and depends upon the solvent polarity. Our current understanding is that, besides vibrational symmetry breaking, the molecular form that is undergoing an asymmetri-

cal charge distribution may also be present. It was shown in Ref. 21 that symmetrical PDs can exist in the ground state as an equilibrium of two forms with symmetrical and asymmetrical charge distributions. An increase of the chain length leads to an increase in the "fraction" of the asymmetrical form, especially in polar solvents. For the shorter molecules, the fraction of molecules with an asymmetrical charge distribution is small, and therefore the shapes of their linear absorption bands do not show a pronounced solvent dependence. However, this fraction of the asymmetrical form can be seen by 2PA measurements owing to the strong effects of symmetry breaking. The 2PA peak spectral position of this form is close to that of the linear absorption peak of the corresponding strongly asymmetrical molecule [for example, compare the first 2PA band in PD 25 with the linear absorption position of the strongly asymmetrical Styryl 1 in Fig. 5(a). Note that $\Delta\mu$ for the asymmetrical form shows a large deviation from the perpendicular to the μ_{01} orientation, which was confirmed by quantum-chemical calculations and two-photon excitation anisotropy measurements. As was already shown in Subsection 3.A and Table 5, the bridged molecular structures, such as PD 200 and PD 2093, are characterized by relatively small values of δ_{2PA} in the first 2PA band compared with their unbridged counterpart PD 2646 and PD 3428. It is reasonable to explain this effect by considering that the introduction of the bridges can protect the molecular structure from this symmetry breaking.

F. One-Photon Excitation Fluorescence Anisotropy

Analysis of one-photon anisotropy $r_{1PA}(\lambda)$ for all symmetrical PDs revealed the alternation of the allowed and forbidden one-photon transitions by symmetry. One-photon forbidden transitions, as transitions between states of the same symmetry, can indicate the possible positions of 2PA bands $1A_1 \rightarrow nA_1$. However, not all $1A_1 \rightarrow nA_1$ transitions are active in 2PA for several reasons. For example, transitions involving orbitals with charge localization at molecular fragments placed
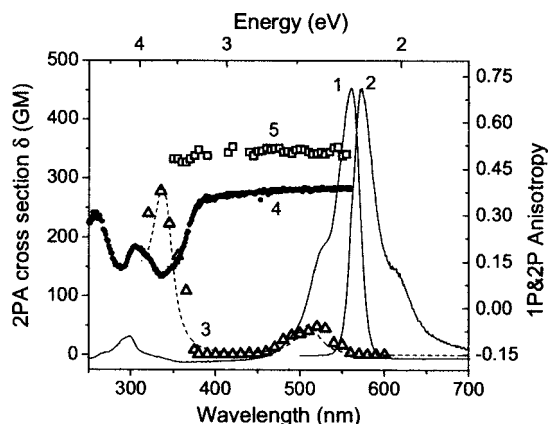
Fig. 7.   Graph of PD 25 in ethanol: 1, linear absorption; 2, fluorescence; 3, 2PA spectra; dashed line, theoretical fitting based on Eq. (2); 4, 5, one- and two-photon excitation anisotropy spectra, respectively, in glycerol. For comparison with linear absorption, 2PA spectra are presented as a function of half the excitation wavelength $\lambda_{exc}/2$.
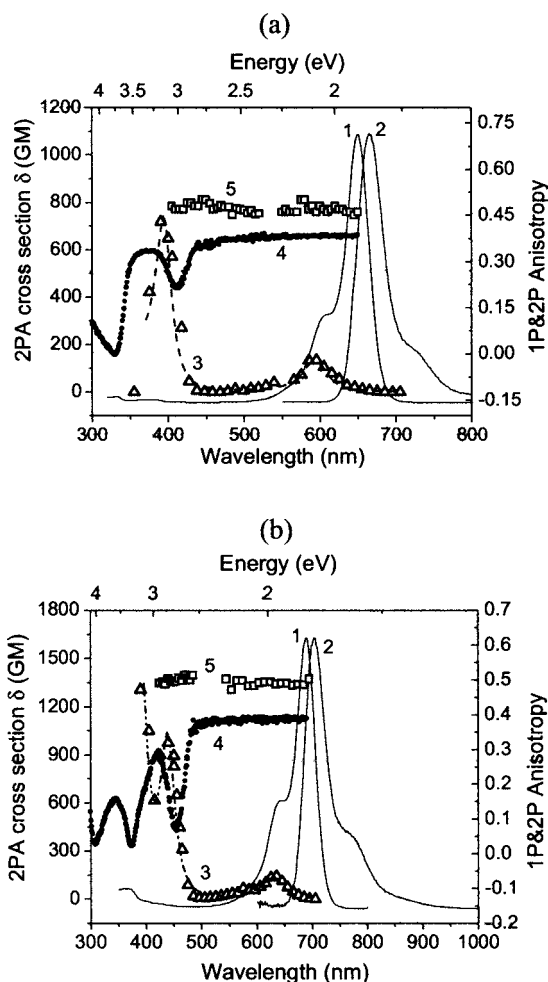
Fig. 8.   (a) PD 2350 in ethanol: 1, linear absorption; 2, fluorescence; 3, 2PA spectra; dashed line, theoretical fitting based on Eq. (2); 4, 5, one- and two-photon excitation anisotropy spectra, respectively, in glycerol, (b) PD 2630 in ethanol: 1, linear absorption; 2, fluorescence; 3, 2PA spectra; dashed line, theoretical fitting; 4, 5, one- and two-photon excitation anisotropy spectra, respectively, in glycerol. For comparison with linear absorption, 2PA spectra are presented as a function of half the excitation wavelength $\lambda_{exc}/2$.

perpendicular to the molecular plane cannot be coupled to the intermediate HOMO and thus cannot be active in 2PA.

In addition, as was mentioned in Subsection 3.E.1, with identical terminal groups there is a splitting of the doubly degenerate local orbitals of the terminal groups that leads to an appearance of two transitions (HOMO−2→LUMO and HOMO−3→LUMO for PD 2350 in Table 6). One of these (HOMO−3→LUMO) can be active in 2PA, and the other (HOMO−2→LUMO) is active in 1PA. The peak of this one-photon transition band should correspond to a dip in the one-photon anisotropy spectrum. The energy splitting depends on the energy position of the orbitals from the isolated terminal groups relative to the chain orbitals and thus upon their structure (length of conjugation, donor strength). A small splitting energy leads to approximate overlap between one-photon anisotropy dips and the positions of the 2PA peaks. Figure 7 shows a strong correlation between the 2PA peak and the one-photon anisotropy dip for PD 25 with thiazolium terminal

groups. The same trend was observed for all thiazolium molecules as well as for squarylium dyes described in Ref. 20. The splitting energy for indolium and benzoindolium dyes is larger. Therefore, for these molecules, the 2PA peaks are blueshifted relative to the anisotropy dips. See examples in Fig. 8. In Fig. 8(a) for PD 2350, the first one-photon anisotropy dip is at 410 nm, which is consistent with the transition HOMO−2→LUMO of wavelength 410 nm as predicted by quantum-chemical calculations. The 2PA peak at 392 nm is consistent with the transition HOMO−3→LUMO of predicted wavelength 395 nm, shown in Table 6.

4. CONCLUSION

We have described a detailed and comprehensive experimental investigation and quantum-chemical analysis of 2PA spectra in a series of cationic polymethines with different molecular structures. From these measurements and analysis we found that in the spectral region between the first absorption band and its double-resonance position there are two 2PA bands. Quantum-chemical analysis allows us to make the following conclusions:

1. For all the molecules investigated, we observed a weakly allowed 2PA band within the short-wavelength shoulder of the first absorption band $S_0 \rightarrow S_1$ when plotted as in, for example, Figs. 2 and 3. This band is only slightly allowed by dipole selection rules for the symmetrical PDs with C_{2v} symmetry; however, it displays 2PA cross section δ_{2PA} up to 600 GM in ethanol owing to the effect of vibrational and charge distribution symmetry breaking. This symmetry breaking effect leads to reorientation of the $\boldsymbol{\Delta\mu}$ dipole difference from perpendicular to $\boldsymbol{\mu}_{01}$ (in this case two-photon excitation fluorescence anisotropy r_{2PA} should be equal to 0.14; see Ref. 21) by an angle of 32° ($r_{2PA} \approx 0.5$).

2. The nature of the strongest 2PA band is connected to the electron transition from HOMO−3, localized on the benzene rings of the terminal groups, to LUMO, which appears in the energy interval between the $S_0 \rightarrow S_1$ absorption band and its double resonance. Relatively high δ_{2PA}, up to 2550 GM, was observed owing to a strong coupling of the boundary orbitals HOMO−3 and LUMO with the intermediate HOMO. Exceptions are PDs 3428 and 2093, whose molecular structures contain phenyl substituents at the nitrogen atoms of the terminal groups. Calculations show that for these molecules, HOMO−3 is localized at the phenyl rings oriented perpendicular to the molecular plane. Therefore, electron transitions involving these orbitals cannot be active in 2PA. The corresponding local orbital, including charge localization at the benzene rings of the terminal groups, becomes HOMO−5, and the 2PA transition is connected with HOMO−5→LUMO.

3. Structure-property relations revealed the following trends:

• an increase of δ_{2PA} upon lengthening of the polymethine chromophore, which is connected with a corresponding increase in the ground-state transition dipole moments and decrease in the detuning energies;

• an increase of δ_{2PA} with increasing donor strength of the terminal groups for dyes of the same chain length;

• a tendency for asymmetrical molecules to show broader and more intense 2PA bands, which are positioned within $S_0 \rightarrow S_1$ absorption.

REFERENCES

1. S. R. Marder, "Organic nonlinear optical materials: where we have been and where we are going," Chem. Commun. (Cambridge) 131–134 (2006).
2. M. Albota, D. Beljonne, J. L. Bredas, J. E. Ehrlich, J.-Y. Fu, A. A. Heikal, S. Hess, T. Kogej, M. D. Levin, S. R. Marder, D. McCord-Maughon, J. W. Perry, H. Rockel, M. Rumi, G. Subramaniam, W. W. Webb, X.-L. Wu, and C. Xu, "Design of organic molecules with large two-photon absorption cross sections," Science **281**, 1653–1656 (1998).
3. T. Kogej, D. Beljonne, F. Meyers, J. W. Perry, S. R. Marder, and J. L. Bredas, "Mechanisms for enhancement of two-photon absorption in donor-acceptor conjugated chromophores," Chem. Phys. Lett. **298**, 1–3 (1998).
4. M. Rumi, J. E. Ehrlich, A. A. Heikal, J. W. Perry, S. Barlow, Z. Hu, D. McCord-Maughon, T. C. Parker, H. Rocker, S. Thayumanavan, S. R. Marder, D. Beljonne, and J. L. Bredas, "Structure-property relationships for two-photon absorbing chromophores: bis-donor diphenylpolyene and bis(styryl)benzene derivatives," J. Am. Chem. Soc. **122**, 9500–9510 (2000).
5. G. S. He, T.-C. Lin, J. Dai, P. N. Prasad, R. Kannan, A. G. Dombroskie, R. A. Vaia, and L.-S. Tan, "Degenerate two-photon-absorption spectral studies of highly two-photon active organic chromophores," J. Chem. Phys. **120**, 5275–5284 (2004).
6. C.-K. Wang, P. Macak, Yi Luo, and H. Agren, "Effects of π centers and symmetry on two-photon absorption cross sections of organic chromophores," J. Chem. Phys. **114**, 9813–9820 (2001).
7. E. Zojer, D. Beljonne, T. Kogej, H. Vogel, S. R. Marder, J. W. Perry, and J. L. Bredas, "Tuning the two-photon absorption response of quadrupolar organic molecules," J. Chem. Phys. **116**, 3646–3658 (2002).
8. E. Zojer, D. Beljonne, P. Pacher, and J. L. Bredas, "Two-photon absorption in quadrupolar π-conjugated molecules: influence of the nature of the conjugated bridge and the donor-acceptor separation," Chem.-Eur. J. **10**, 2668–2680 (2004).
9. R. S. Lepkowicz, O. V. Przhonska, J. M. Hales, D. J. Hagan, E. W. Van Stryland, M. V. Bondar, Yu. L. Slominsky, and A. D. Kachkovski, "Excited-state absorption dynamics in polymethine dyes detected by polarization-resolved pump–probe measurements," Chem. Phys. **286**, 277–291 (2003).
10. J. M. Hales, D. J. Hagan, E. W. Van Stryland, K. J. Schafer, A. R. Morales, K. D. Belfield, P. Pacher, O. Kwon, E. Zojer, and J. L. Bredas, "Resonant enhancement of two-photon absorption in substituted fluorene molecules," J. Chem. Phys. **121**, 3152–3160 (2004).
11. M. Hamer, *The Cyanine Dyes and Related Compounds* (Interscience, 1964).
12. J. R. Lakowicz, *Principles of Fluorescence Spectroscopy* (Kluwer Academic/Plenum, 1999).

13. M. Sheik-Bahae, A. A. Said, and E. W. Van Stryland, "High-sensitivity, single-beam n_2 measurements," Opt. Lett. **14**, 955–957 (1989).

14. C. Xu and W. W. Webb, "Measurement of two-photon excitation cross sections of molecular fluorophores with data from 690 to 1050 nm," J. Opt. Soc. Am. B **13**, 481–491 (1996).

15. M. Sheik-Bahae, A. A. Said, T.-H. Wei, D. R. Hagan, and E. W. Van Stryland, "Sensitive measurement of optical nonlinearities using a single beam," IEEE J. Sel. Top. Quantum Electron. **26**, 760–769 (1990).

16. M. Fisher and J. Georges, "Fluorescence quantum yield of Rhodamine 6G in ethanol as a function of concentration using thermal lens spectrometry," Chin. Phys. Lasers **260**, 115–118 (1996).

17. J. Fu, O. V. Przhonska, L. A. Padilha, D. J. Hagan, E. W. Van Stryland, K. D. Belfield, M. V. Bondar, Yu. L. Slominsky, and A. D. Kachkovski, "Two-photon anisotropy: analytical description and molecular modeling for symmetrical and asymmetrical organic dyes," Chem. Phys. **321**, 257–268 (2006).

18. M. J. S. Dewar, *The Molecular Orbital Theory of Organic Chemistry* (McGraw-Hill, 1969).

19. J. S. Craw, J. R. Reimers, G. B. Bacskay, A. T. Wong, and N. S. Hush, "Solitons in finite- and infinite-length negative-defect *trans*-polyacetylene and the corresponding Brooker (polymethinecyanine) cations," Chem. Phys. **167**, 77–99 (1992).

20. J. Fu, O. V. Przhonska, L. A. Padilha, D. J. Hagan, E. W. Van Stryland, M. V. Bondar, Yu. L. Slominsky, and A. D. Kachkovski, "Experimental and theoretical approaches to understanding two-photon absorption spectra in polymethine and squaraine molecules," J. Opt. Soc. Am. B **24**, 67–76 (2007).

21. R. S. Lepkowicz, O. V. Przhonska, J. M. Hales, J. Fu, D. J. Hagan, E. W. Van Stryland, M. V. Bondar, Yu. L. Slominsky, and A. D. Kachkovski, "Nature of the electronic transitions in thiacarbocyanines with a long polymethine chain," Chem. Phys. **305**, 259–270 (2004).

22. K. Kamada, K. Ohta, Y. Iwase, and K. Kondo, "Two-photon absorption properties of symmetric substituted diacetylene: drastic enhancement of the cross section near the one-photon absorption peak," Chem. Phys. Lett. **372**, 386–393 (2003).

23. D. Scherer, R. Dorfler, A. Feldner, T. Vogtmann, M. Schwoerer, U. Lawrentz, W. Grahn, and C. Lambert, "Two-photon states in squaraine monomers and oligomers," Chem. Phys. **279**, 179–207 (2002).